

Plasmons on Wide Epitaxially-grown Quantum Wells*

John F. Dobson

Faculty of Science and Technology,
Griffith University, Nathan, Qld 4111, Australia.

Abstract

Quantum wells can now be grown by molecular beam epitaxy in the $\text{Ga}_{1-x}\text{Al}_x\text{As}$ system with almost any desired electron confinement potential $V(z)$ in the growth or z direction. The wells can be filled by remote doping, giving finely controllable high-mobility electron gases with a dimensionality between two and three. Grating coupler techniques permit observation at finite surface wavenumber of the infrared plasmon modes of these structures. This provides in principle a window onto fundamental and applicable many-electron physics. Of special interest are the ‘pseudo-jellium’ properties of parabolic and parabolic-linear wells, which are discussed in detail here. A theorem applicable to more general wells is also introduced.

1. Introduction

The technique of molecular beam epitaxy (MBE) permits growth, atomic layer by layer, of high-quality GaAs crystals. Addition of aluminium to the process leads to crystals of $\text{Ga}_{1-x}\text{Al}_x\text{As}$ in which the aluminium fraction x can be controlled during growth. Thus x is a specified function $x(z)$ of the position variable z measured in the crystal growth direction (Sundaram *et al.* 1988; Gwinn *et al.* 1989). Since the bandgap ϵ_g and hence the conduction-band minimum ϵ_c of this direct-gap semiconductor system depend on the aluminium fraction x , one can grow layered samples with a chosen spatial profile $\epsilon_c(z)$. Within the envelope function approximation (Bastard 1981; Burt 1992), the spatially varying energy $\epsilon_c(z)$ takes the role of an external potential energy function $V_{\text{bare}}(z)$. Electron transport is then governed by a Schrödinger equation for an envelope wavefunction describing the motion of electron wavepackets with effective mass m^* , confined in the z direction by the ‘potential’ $V_{\text{bare}}(z)$ plus their own self-consistent electrostatic field, but free to move in the x and y directions parallel to the epitaxial layers. At any given position z , the effective mass m^* is determined in the usual way by the k -space curvature of the conduction-band dispersion $\epsilon(\mathbf{k})$ at the Brillouin zone centre $\mathbf{k} = 0$. A slight complication arises because the spatially varying Al content also gives rise to a spatial variation of the effective mass and of the semiconductor’s dielectric constant. For the experiments we consider these effects are of the order of 10% and we will ignore them for the bulk of the present discussion.

* Paper presented at the Gordon Godfrey Workshop, University of New South Wales, Sydney, 20–21 July 1992.

One familiar case of a $\text{Ga}_{1-x}\text{Al}_x\text{As}$ quantum well is that formed at a relatively abrupt heterojunction between GaAs ($x = 0$) and GaAlAs (Stern and Das Sarma 1984). Here the effective bare external potential $V_{\text{bare}}(z)$ introduced above has a step-function dependence on z . Motion of electrons in the potential leads to self-consistent space charge with consequent band bending, and the effective total potential $V_{\text{eff}}(z)$ has a linear ‘notch’-shaped minimum. Electrons supplied by spatially remote doping ‘fall’ into this potential minimum, where they form a quasi-two-dimensional electron gas.

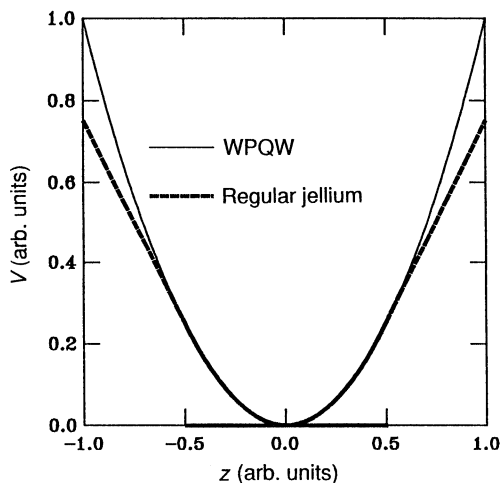


Fig. 1. Comparison of bare positive background potentials for a finite thickness of regular jellium (thick dashed curve) and for a finite thickness of ‘embedded electron gas’ as in a wide parabolic quantum well (thin curve). The region of positive background in the regular jellium case is shown as a heavy line on the horizontal axis. The positive background extends to $\pm \infty$ in the non-neutral embedded (WPQW) case. [From Dobson (1992).]

In addition to such abrupt interfaces, it is possible to grow wells having an essentially continuous variation of Al content with z . A case of particular interest here is the *parabolic quantum well* (PQW), for which $V_{\text{bare}}(z) = \frac{1}{2}\kappa z^2$ (see the thin curve in Fig. 1). This case is special because a wide slab of uniform positive background of charge density $n_0 e$ per unit volume produces, by Poisson’s equation, an electron potential energy $V_{\text{bare}}(z) = \frac{1}{2}n_0 e^2 \epsilon^{-1} z^2$. Thus by growing a parabolic well of curvature κ one has effectively formed a uniform ‘jellium’ positive background with charge density $n_0 e = \epsilon \kappa / e$. Conduction electrons produced by spatially remote doping form a high-mobility gas in this normally empty well (Sundaram *et al.* 1988).

The properties of an electron gas moving through a uniform jellium background have been the subject of a large amount of theoretical work over many years (Ceperley and Alder 1980; Mahan 1981; Green *et al.* 1985). The original reason for this interest is that the jellium model is a first approximation to the conduction electron system of the ‘simple’ (s-p bonded) metals, in which the effects of the discrete ionic lattice structure on the conduction electrons are fairly weak. The

geometrical simplicity of the jellium problem has allowed much progress to be made with the difficult problem of electron–electron interactions. Even when the translational symmetry is broken by the presence of a surface, the local density functional approximation (LDA) (Kohn and Sham 1965; Dreizler and Gross 1990) has allowed nontrivial calculation of electron gas properties (Lang and Kohn 1970; Lang 1973; Feibelman 1982; Rose and Dobson 1981; Dobson and Harris 1983, 1988; Eguiluz 1983; Liebsch 1987). The sophistication of both jellium theory and experimentation on the simple metals and their surfaces (vom Felde *et al.* 1989; Tsuei *et al.* 1991) has now reached a point where further progress on the many-body problem will probably require the inclusion of the detailed effects of discrete ions, a daunting prospect for the theorist.

An alternative approach is suggested by the availability of wide parabolic wells in the $\text{Ga}_{1-x}\text{Al}_x\text{As}$ system. As shown above, the high-mobility electron gas in these wells should be an analogue of the jellium electron gas. Furthermore, at typical experimentally achievable electron densities, both the Fermi wavelength λ_F and the Thomas–Fermi screening length λ_{TF} greatly exceed the underlying semiconductor lattice spacing. By contrast, in a real simple metal (e.g. Al, Na, Mg), λ_F and λ_{TF} are both comparable to the lattice spacing, so ‘grainy’ lattice effects on electron gas properties are more significant.

In short, epitaxial parabolic quantum wells promise to be a ‘better’ jellium electron-gas system on which to test existing many-body theories, than are the simple metals for which the theories were originally formulated. The only modification required to the jellium model, to a first approximation, is to use the conduction band effective mass m^* and a background semiconductor dielectric constant ϵ which are very different from the free-space values. Some typical numbers for $\text{Ga}_{1-x}\text{Al}_x\text{As}$ are as follows: dielectric constant $\epsilon/\epsilon_0 \approx 13.1$; effective mass $m^*/m \approx 0.069$; effective Bohr radius $a_B^* = \hbar^2\epsilon/m^*e^2 \approx 100 \text{ \AA} \gg$ lattice spacing. For much of what follows we will use ‘starred’ Hartree units, a.u.* for which $e^2/\epsilon = 1$, $m^* = 1$, $\hbar = 1$. Thus the unit of energy or angular frequency is $1 \text{ a.u.}^* = 1 \text{ Hartree}^* = 11 \text{ meV} = 1.7 \times 10^{-21} \text{ J}$, equivalent to a photon with reciprocal wavelength $9.0 \times 10^3 \text{ m}^{-1}$ (in the far infrared). The unit of length is $1 \text{ a.u.}^* = a_B^* = 1.0 \times 10^{-8} \text{ m}$. For a grown effective density (as in Pinsukanjana *et al.* 1992) of $n_0 = 2.75 \times 10^{22} \text{ m}^{-3}$, we have an inter-electron spacing $r_s = 2.07 a_B^*$ (analogous to aluminium), $\lambda_F = 2\pi/k_F \approx 677 \text{ \AA}$, $\lambda_{TF} = 2\pi/q_{TF} \approx 578 \text{ \AA}$, $\omega_p = 0.581 \text{ a.u.}^* \equiv 5.2 \times 10^3 \text{ m}^{-1}$.

Fig. 2 shows an experimental setup (Pinsukanjana *et al.* 1992) for measuring the response of a wide quantum well to electromagnetic excitation in the far

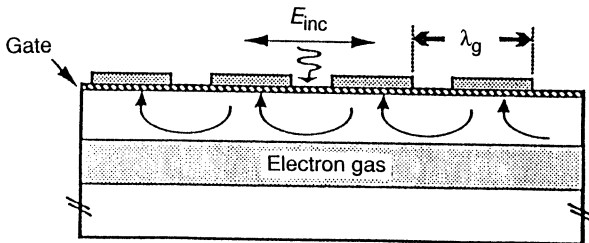


Fig. 2. Experimental arrangement for far-infrared grating coupler experiments on a wide quantum well in $\text{Ga}_{1-x}\text{Al}_x\text{As}$. [Modified from Pinsukanjana *et al.* (1992).]

infrared region. A thin (semi-transparent) metal gate is used to set a d.c. bias relative to a side contact on the electron gas, and so attract a predetermined areal density of electrons into the electron gas layer. By variation of this gate bias a given sample can be converted from a truly ‘two-dimensional’ electron gas with only one sub-band lightly occupied, through to a thick electron layer with several sub-bands occupied, and therefore approaching a three-dimensional nature. A thick metal grating of spacing λ_g is laid on top of the gate at position z_g . When irradiated normally with infrared (IR) radiation it produces near-field components with surface-parallel wavenumbers $2\pi n/\lambda_g$, to which the trapped electron layer responds. Peaks in transmission, reflection or absorption indicate a natural mode frequency of the electron gas.

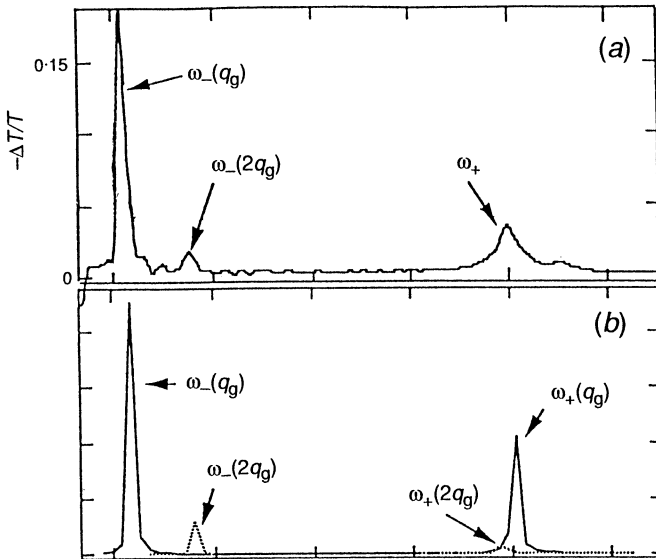


Fig. 3. (a) IR transmission data (percentage power transmission) obtained with the apparatus of Fig. 2 for a pure parabolic quantum well with $r_s^* = 2.07$ and electron layer thickness 8.8 a.u.^* (b) Theoretically predicted power absorption for the above experimental data, from time-dependent local density functional calculations (see Section 7). [Modified from Pinsukanjana *et al.* (1992).]

In the experiment shown (Pinsukanjana *et al.* 1992) the percentage variation in infrared transmission $\Delta T/T$ of the $r_s^* = 2.07$ sample was measured (see Fig. 3a). It showed two strong resonances, near ω_p and $\omega_{2D}(2\pi/\lambda_g)$ respectively, where $\omega_p = (n_0 e^2/\epsilon m^*)^{1/2}$ is the 3D plasma frequency and $\omega_{2D}(q) = (N_s e^2 q/2\epsilon m^*)^{1/2}$ is the 2D plasma frequency (see also Sections 2 and 3). There is also a third, weaker, resonance near $\omega_{2D}(4\pi/\lambda_g)$. In Sections 3 and 5 we shall see why, under irradiation with a grating coupler giving low surface-parallel wavenumbers, these are the only strong resonances of a parabolic well. This is confirmed by the numerical absorption predictions (Fig. 3b) made by the author from the theory of Section 7 below.

The discussion above might appear to suggest that a wide parabolic quantum well (WPQW), partially filled with electrons, should be a perfect analogue of

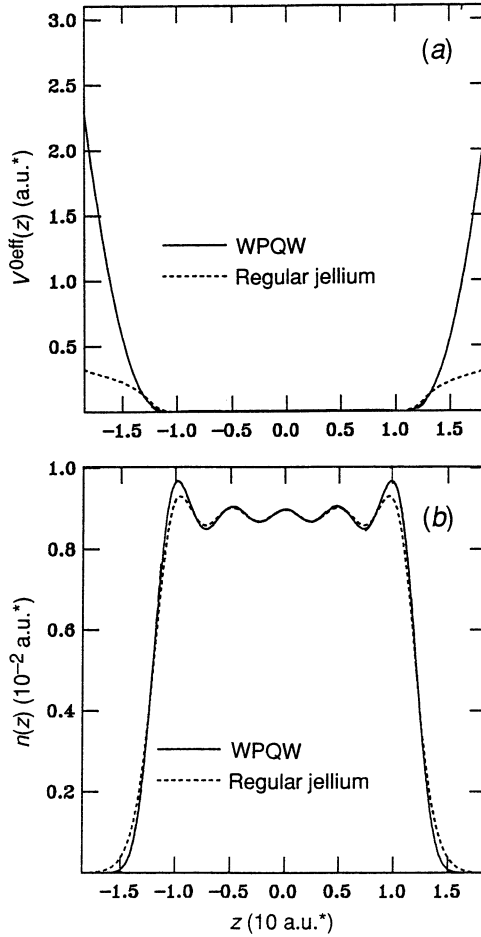


Fig. 4. (a) Self-consistent ground-state Kohn–Sham potential in a regular neutral jellium slab (dotted curve) and a non-neutral embedded jellium slab (WPQW, solid curve). Nominal electron gas width L is 25 a.u.* and $r_s^* = 3$. Five sub-bands are occupied. (b) Self-consistent ground-state electronic charge density $n(z)$ in a neutral jellium slab (dotted) and a WPQW (solid), for the same well as Fig. 4a.

a slab of jellium metal of finite thickness. This is not in fact the case: in a finite electrically neutral slab of jellium, the parabolic external potential extends only to the edge of the positive background, outside which it is replaced by a gradient-matched *linear* potential satisfying Poisson’s equation with zero charge density (Fig. 1, thick line). When filled to charge neutrality with electrons, the neutral jellium slab has a total self-consistent potential which asymptotes to a constant as $z \rightarrow \pm \infty$, thus permitting definition of a work function ϕ (see Fig. 4a, dotted curve). By contrast, in a typical WPQW the bare potential (Fig. 1, thin curve) continues to grow parabolically outside the region occupied by electrons. The system is effectively non-neutral, so that the total self-consistent potential, while relatively flat inside the electron gas layer, rises quadratically

outside the layer (Fig. 4*a*, solid curve). Far from the electron layer the grown parabola flattens off because of practical chip design considerations, but doping and bias regimes can be chosen so that this occurs well outside the electron gas layer. In more pictorial terms, the difference between a neutral jellium slab and a WPQW device is summarised in Fig. 5, which shows how the electron gas is ‘embedded’ deep inside the positive background in the WPQW case, in contrast to the regular neutral jellium case where the edges of the electron gas and of the positive background coincide. The electron density is fairly uniform inside either a WPQW or a regular jellium (Fig. 4*b*) but the electron gas surface is different in the two cases.

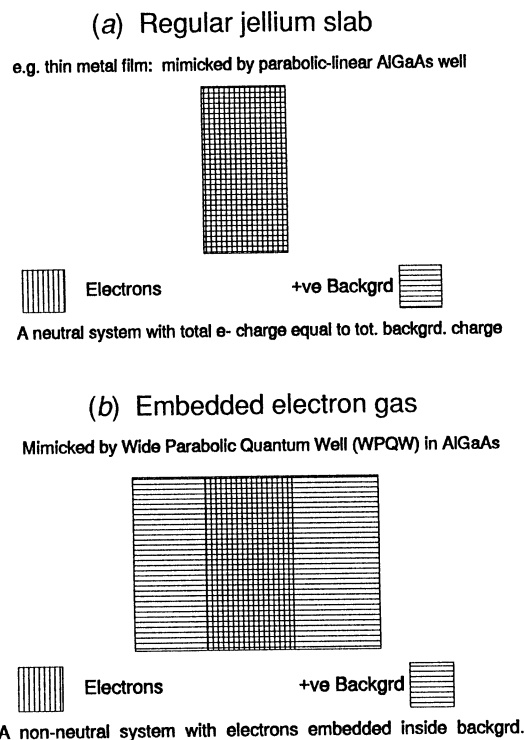


Fig. 5. (a) Schematic view of electron charge distribution (vertical hatching) and positive background charge distribution (horizontal hatching) in a neutral jellium slab. (b) As in (a) but for an embedded electron gas layer (non-neutral jellium, WPQW).

In due course we will show that, at least for spatially homogeneous m^* and ϵ , the infrared spectrum of a pure parabolic well, for experimentally achievable surface-parallel wavenumbers much less than k_F , is not particularly revealing about fundamental issues in many-electron physics, being constrained by two theorems. However, the same considerations also show that if one uses larger wavenumbers, or grows a parabolic well with a linear lip or lips, then a richer spectrum occurs which may shed more light on fundamental issues. By the discussion of the previous paragraph, this parabolic-linear configuration is seen

to mimic a true jellium slab, provided suitable gate bias is supplied to ensure a 'neutral' jellium edge.

The remainder of this paper is set out as follows. In Section 2, a simple hydrodynamic treatment is given which qualitatively describes, at small wavenumber, the collective electronic modes of (a) a bulk 3D electron gas; (b) a bulk 2D electron gas; (c) a halfspace of 3D electron gas (giving surface plasmons); and (d) a finite slab of electron gas. For the finite slab we find modes which are surface plasmons for large surface wavenumber q_{\parallel} , one of which has a 2D plasmon-like dispersion at small q_{\parallel} . There are also standing bulk plasma waves fitting across the slab.

It is also argued that more sophisticated hydrodynamic models with diffuse surfaces should yield an additional mode or modes, the multipole surface plasmons. Clearly this hydrodynamic approach misses peaks in the infrared response which are due to transitions between particular quantum eigenstates of the confined z -motion. In the case of wide parabolic and near-parabolic wells, however, single-particle modes turn out to be less prominent than one might have expected, because of level crowding and Landau damping. Nevertheless, a more complete description will treat the quantum many-body nature of the response problem, and this is addressed in the following sections.

In Section 3 we turn to the special case of an exactly parabolic quantum well, summarising a Kohn-theorem argument (Brey *et al.* 1989) to show that for excitation with a spatially uniform finite-frequency electric field directed in the z (quantum confinement) direction, a resonance occurs at exactly the bulk plasma frequency $(n_0 e^2/\epsilon m^*)^{1/2}$, irrespective of the electron gas width. This result is also independent of the detailed form of the interaction between electrons. The relevance to IR grating coupler experiments is discussed, and it is argued that such a peak does appear in the data of Pinsukanjana *et al.* (1992) (Fig. 3a).

To investigate other IR absorption phenomena at a level beyond hydrodynamics, one must set up a microscopic description of quantum-mechanical motion of electrons in a total potential consisting of external, self-consistent Hartree and exchange-correlation contributions. The relevant theory is outlined in Section 4, using local density functional theory to handle the exchange and correlation phenomena.

In Section 5, it is shown analytically, within a rather general class of approximations for exchange and correlation, that all quantum wells with a 1D confining potential and free motion in the two other dimensions, however wide, complicated or highly populated, and at any temperature, exhibit a '2D plasmon' oscillation mode with frequency $\omega = (N_s \epsilon^2 q_{\parallel}/\epsilon m)^{1/2}$. Here N_s is the well population in electrons per unit area, q_{\parallel} is the surface-parallel wavenumber of the mode, and the dielectric constant ϵ and effective mass m^* are assumed spatially homogeneous and isotropic. The above result holds when $q_{\parallel} W \ll 1$, where all electron density (including the dynamically excited part) is confined to a region of width W . This result is somewhat more general than others appearing in the literature: along with the Kohn theorem of Section 3, it accounts completely for the observed low- q_{\parallel} IR spectrum, up to about the bulk plasma frequency, of a pure parabolic quantum well.

For quantum wells which are not exactly parabolic, or for higher surface-parallel wavenumbers such that the theorems of Sections 3 and 5 do not apply, it is

necessary to perform numerical calculations to predict the IR spectrum. These are reviewed in Section 6, where the two basic approaches are compared:

- (a) an eigenfunction basis-set approach wherein, at least for low numbers of occupied sub-bands and unevenly spaced levels, the modes divide into ‘intra-band’ (low-frequency) and ‘inter-band’ (high-frequency) groupings; and
- (b) a real-space (z, z') formalism emphasising the spatial distribution $\Delta n(z)$ of oscillating charge density, and relating more directly to the simple hydrodynamic approach reviewed in Section 2.

The two formalisms, when correctly converged, give the same answers, including the phenomena of single-particle (particle-hole) resonances, collective resonances and Landau damping, but some phenomena are more readily understood qualitatively in one formalism than in the other.

In Section 7, using the real-space formalism, the IR spectra of parabolic and linear-parabolic wells are investigated numerically, and it is shown that linear-parabolic wells (mimicking a true jellium slab) should have multipole surface plasmon modes which do not occur for pure parabolic wells.

Finally, in Section 8 the above discussion is summarised, and the prospects for future theoretical, experimental and device-oriented work is discussed.

2. Qualitative Expectations from Hydrodynamics

A dispersive hydrodynamic model (Jackson 1962) is the simplest formalism able to tie together the collective behaviours of bulk 3D and 2D electron gases, as well as various known simple-metal surface effects such as monopole and (at least qualitatively) multipole surface plasmons (Bennett 1970; Eguiluz *et al.* 1975; Eguiluz and Quinn 1976; Das Sarma and Quinn 1979; Mahanty 1982; Schwartz and Schach 1982, 1984). We also use it here for a qualitative picture of standing plasmon resonances and coupled surface excitations of finite jellium slabs. A detailed account was given in Eguiluz (1979).

The variables used in this approach are the electron gas density perturbation $n(\mathbf{r}, t)$ and the fluid velocity $\mathbf{u}(\mathbf{r}, t)$. By eliminating \mathbf{u} between linearised continuity (electron number conservation) and Euler ($F = m\mathbf{a}$) equations one obtains a second-order differential equation for the density perturbation $n(\mathbf{r}) \exp(-i\omega t)$ in a region of uniform background density n_0 :

$$\beta^2 \nabla^2 n + \omega(\omega + i\tau^{-1}) n = -n_0 m^{-1} \nabla^2 \phi. \quad (1)$$

Here τ is a phenomenological Drude damping time and ϕ is a total electron potential energy perturbation. The ‘pressure’, ‘dispersion’ or ‘diffusion’ coefficient β has dimensions of velocity and arises from an assumed force $-\beta^2 \nabla n/n_0$ in the Euler equation. The conventional value $\beta^2 = 0.6v_F^2 = 0.6\hbar^2 m^{-2} (3\pi^2 n_0)^{2/3}$ for plasmons in degenerate electron gases is usually justified by comparison of the predictions of (1) with those of the finite-frequency microscopic Lindhard response function (Mahan 1981) in the limit of small wavenumbers. Correspondingly, the hydrodynamic theory is most plausible for phenomena varying slowly in space.

In the simplest (mean-field) approach, ϕ is the total electron potential energy due to the electron number density perturbation n , plus any external source:

$$\phi = V_C * n + \phi^{\text{ext}}. \quad (2)$$

Here the asterisk represents convolution in real space, V_C is the bare Coulomb potential whose space Fourier transform $V_C(q)$ is $e^2/\epsilon q^2$ in 3D and $e^2/2\epsilon q$ in 2D, and ϵ is the background dielectric function of the medium (e.g. GaAs) through which the electrons move.

(2a) *Plasmons in Bulk 3D and 2D Systems*

We can combine (2) and (1) for the case of an unforced ($\phi^{\text{ext}} = 0$) wavelike density disturbance with $n = \exp(i\mathbf{q} \cdot \mathbf{r} - i\omega t)$. This gives the hydrodynamic dispersion relation for 3D bulk plasmons when $\omega_p \tau \gg 1$ as

$$\omega_{3\text{DP}}^2 = \omega_p^2 + \beta^2 q^2 - i\omega_p \tau^{-1}, \quad \omega_p^2 = n_0 e^2 / \epsilon m. \quad (3)$$

Similarly, the plasmon dispersion for a 2D electron gas of infinite extent in the limit $\omega_{2\text{D}} \tau \gg 1$ is predicted to be

$$\omega_{2\text{DP}}^2 = \omega_{2\text{D}}^2 + \beta^2 q^2 - i\omega_{2\text{D}} \tau^{-1}, \quad \omega_{2\text{D}}^2 = N_s e^2 q / 2\epsilon m. \quad (4)$$

Here N_s is the traditional 2D notation for the electron number n_0 per unit area. Of particular note is the \sqrt{q} dependence of the 2D plasmon frequency $\omega_{2\text{D}}$ in the limit $q \rightarrow 0$, $\tau \rightarrow \infty$, compared with the finite 3D plasma frequency as $q \rightarrow 0$.

(2b) *Plasmons at the Surface of a Three-dimensional Electron Gas*

We assume that the electron gas occupies the half-space $z < 0$. In addition to reflecting incident 3D plasmons, the surface can support surface plasmons whose oscillating density disturbance is wavelike in the x direction parallel to the surface but decays exponentially into the bulk (Ritchie 1957): thus $n(x, z, t) = \text{const.} \exp(Qz + iq_{\parallel} x - i\omega t)$. Boundary conditions are needed for the hydrodynamic Euler equation. The simplest assumption is that the surface-normal fluid velocity vanishes at the surface, $u_z(z=0) = 0$: this will be termed the 'hard-wall' condition. Assuming that $n(z)$ is zero for $z > 0$, and that the electric field and potential are continuous at the surface, one finds (Mahanty 1982; Schwartz and Schaich 1982) a surface plasmon frequency

$$\omega = \frac{\omega_p}{\sqrt{2}} (\sqrt{1+x^2} + x), \quad x \equiv \beta q_{\parallel} / \sqrt{2} \omega_p, \quad (5)$$

which approaches $\omega_p / \sqrt{2}$ as $q_{\parallel} \rightarrow 0$. The inverse penetration depth is

$$Q = -q_{\parallel} / 2 + (0.25 q_{\parallel}^2 + 0.5 \omega_p^2 \beta^{-2})^{1/2}, \quad (6)$$

which approaches $\omega_p / \sqrt{2} \beta$ as $q_{\parallel} \rightarrow 0$: this is of order q_{TF} , the Thomas-Fermi wavenumber.

The conclusion that $\omega \rightarrow \omega_p / \sqrt{2}$ as $q_{\parallel} \rightarrow 0$ is borne out by more sophisticated treatments of the bounded electron gas problem, and is independent of surface details (Harris and Griffin 1971; Feibelman 1971). The positive dispersion predicted by (5) is, however, an artifact of the hydrodynamic and hard-wall approximations made here: for example, the initial ($q_{\parallel} \rightarrow 0$) dispersion of surface plasmons on simple metal surfaces is found both experimentally (Tsuei *et al.* 1991) and in more complete theories (Feibelman 1982; Liebsch 1987) to be negative.

(2c) *Dispersive Hard-wall Hydrodynamic Model for Electron Gas Slab*

A simple model for a slab of electron gas with finite thickness L can be made from the dispersive hydrodynamics already presented, with hard walls at $z = \pm L/2$ and an electron density perturbation of the form $n(z) \exp(iq_{\parallel} x - i\omega t)$, and with $n(z)$ zero for $|z| > L/2$ (Eguiluz 1979). Free (undriven) plasmon solutions can be divided into even and odd categories with density profiles as follows:

$$n(z) = \cosh(Qz) \theta(L/2 - |z|) \quad (\text{even solution}), \quad (7)$$

$$= \sinh(Qz) \theta(L/2 - |z|) \quad (\text{odd solution}). \quad (8)$$

We first discuss solutions with real Q , corresponding to coupled surface plasmon modes in which the disturbance is localised near the surfaces, with inverse penetration depth Q . There are also standing-wave (cosine and sine) solutions corresponding to (7) and (8) but with imaginary Q : these will be discussed later.

We assume $e\partial\phi/\partial z - m\beta^2 n_0^{-1} \partial n/\partial z = 0$ at $z = \pm L/2$ [equivalent to Euler's equation with $u_z(z = \pm L/2) = 0$]. Then, using Poisson's equation with electric field and potential continuous at both surfaces, we obtain an equation for the inverse penetration depth Q in the even surface-plasmon case corresponding to equation (7):

$$q_{\parallel} \tanh(q_{\parallel} L/2) = Q \tanh(QL/2) \left(1 + \frac{2\beta^2}{\omega_p^2} \frac{q_{\parallel}^2 - Q^2}{1 + e^{-q_{\parallel} L}} \right). \quad (9a)$$

In the odd case corresponding to (8), equation (9a) is replaced by

$$q_{\parallel} \coth(q_{\parallel} L/2) = Q \coth(QL/2) \left(1 + \frac{2\beta^2}{\omega_p^2} \frac{q_{\parallel}^2 - Q^2}{1 - e^{-q_{\parallel} L}} \right). \quad (9b)$$

The dispersion relation in both cases is

$$\omega(\omega + i\tau^{-1}) = \omega_p^2 + \beta^2(q_{\parallel}^2 - Q^2), \quad (10)$$

which is simply the bulk dispersion relation with an imaginary wavenumber $\pm iQ$ in the z direction.

Equations (9) always have the solutions $Q = \pm q_{\parallel}$ which are in fact spurious for the case $\{\beta \neq 0, L \text{ finite}\}$ since they make the potential infinite. The other solutions are admissible.

For thick slabs ($L \rightarrow \infty$) the \tanh factors in (9a) are unity and after cancelling a factor $(Q - q_{\parallel})$ we recover (6) which relates Q to q_{\parallel} for a single surface. Thus from (10) we recover the surface plasmon dispersion relation (5) as for a semi-infinite slab. The interpretation is that, for thick slabs, the surface plasmon modes of the two surfaces are decoupled because the Coulomb interaction between two sheets of wavelike charge distribution, separated by a distance $z = L$, falls off as $\exp(-q_{\parallel} L)$.

In the long-wavelength limit, $q_{\parallel} L \ll 1$, the left side of (9a) is of order q_{\parallel}^2 so that the term in the large parentheses on the right vanishes to $O(q_{\parallel})$, giving

$$\beta^2(q_{\parallel}^2 - Q^2) = \omega_p^2(-1 + q_{\parallel} L/2 \dots). \quad (11)$$

Thus the leading term in (10) is the 2D plasmon relation (4). Hence in this model it is *not* necessary to have a thin (two-dimensional) electron gas in order to obtain the 2D plasmon dispersion relation: it is sufficient that the wavelength along the surface be much greater than the slab thickness. Like the $q_{\parallel} \rightarrow 0$ limit of the surface plasmon dispersion relation discussed earlier, this is also a universal result, not restricted to the hydrodynamic model or to hard-wall boundary conditions, as will be seen later in this article. Despite the 2D form of the dispersion relation in the case $q_{\parallel} L \ll 1$, the spatial distribution of oscillatory density in the present model is not two-dimensional. Equation (11) shows that $Q \sim \omega_p/\beta \sim q_{TF}$ so that, from (7), the plasmon charge density for a thick slab ($q_{TF} L \gg 1$) resides in a layer roughly one Thomas–Fermi screening length wide on each side of the slab, corresponding to coupled surface plasmons. This will also be borne out later by more complete calculations.

The odd surface-plasmon solution is obtained from (9b). Once again the solutions $Q = \pm q_{\parallel}$ are spurious for $\beta \neq 0$ when L is finite, but the other real solution for Q is valid and when inserted into (10) gives a dispersion relation. The thick-slab limit $q_{\parallel} L \gg 1$, $q_{TF} L \gg 1$ gives once again the single-surface plasmon dispersion relation (5), indicating electrical decoupling between two out-of-phase surface plasmons.

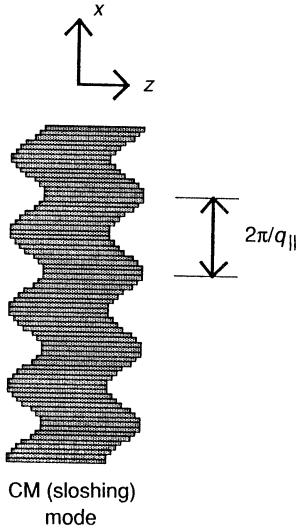


Fig. 6. Qualitative snapshot of the dynamic electronic density distribution in a sloshing mode (centre-of-mass mode, odd ripplon) on a jellium slab.

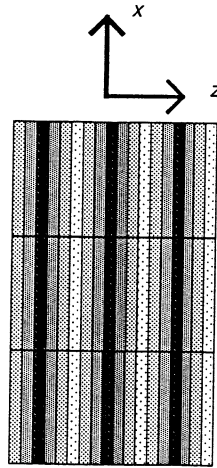
The thin-slab limit of equation (9b) is more delicate than for the even modes described by (9a). When $q_{\parallel} = 0$ it is readily shown that the only real solution of (9b) has $Q = 0$ which, from (8), corresponds to an unacceptable null density disturbance. In fact there is a minimum q_{\parallel} value, called by Eguiluz (1979) the critical wavenumber q_c , such that the odd-surface-plasmon condition (9b) yields a real penetration wavenumber Q . When $q_{\parallel} < q_c$ the odd mode does not disappear, however, but changes to an odd standing-bulk-plasmon mode which

in effect has an imaginary penetration wavenumber, $Q = ik$: this type of solution is discussed in the next paragraph. This behaviour leads to a single continuous mode which changes from standing-wave character to surface-plasmon character as q_{\parallel} increases through q_c . The dispersion relation is smooth and shows no anomaly at $q_{\parallel} = q_c$. This mode is related to the ‘sloshing’ excitation shown in Fig. 6.

We turn now to the even and odd standing-wave plasmon solutions obtained from equations (9a) and (9b) by setting $Q = ik$ throughout, where k is real. In this case the density has spatial oscillations in the z direction, representing standing plasma waves fitting across the slab (Fig. 7). The $u_z = 0$ boundary condition allows discrete wavenumbers $k = M\pi/L$. For $q_{\parallel} \neq 0$, M takes discrete *but non-integral* values. Using (10) we obtain the dispersion of standing bulk plasma waves across the slab:

$$\omega(\omega + i\tau^{-1}) = \omega_p^2 + \beta^2[(M\pi/L)^2 + q_{\parallel}^2]. \quad (12)$$

Equation (12) is readily understood as the bulk dispersion relation (3) with a wavenumber $\mathbf{q} = q_{\parallel} \hat{\mathbf{x}} + (M\pi/L) \hat{\mathbf{z}}$.



Standing plasmon
(case $q_{\parallel} = 0$)

Fig. 7. Qualitative snapshot of the electronic charge distribution in a bulk standing wave plasmon mode fitting across the slab width L .

(2d) Omissions of the Hard-wall Hydrodynamic Model

The assumption of the hard-wall boundary condition $u_z = 0$, and of a sharp electron gas surface, is mathematically convenient, giving rise to near-analytic solutions as discussed in Sections 2b and 2c above. This simplified boundary condition does lead to the loss of some interesting physics, however. A case in point is the multipole surface plasmon (Bennett 1970; Schwartz and Schaich 1984; Dobson and Harris 1988; Tsuei *et al.* 1991). Its existence can be surmised

qualitatively along the following lines. For frequencies below the bulk plasma frequency, equation (3) shows that bulk 3D plasmons are evanescent (q_z is imaginary). If a smoothly-falling surface density $n_0(z)$ (a 'selvage') is present, standing plasmons with frequency below the bulk ω_p but above the local plasma frequency $[n_0(z)e^2/\epsilon m]^{1/2}$ may become trapped in the selvage since they cannot propagate into the bulk. Such standing modes require a sufficiently wide selvage. There is an extensive literature on multipole surface plasmons (Tsuei *et al.* 1991), which have now been seen experimentally at a frequency near $0.8 \omega_p$ on the surfaces of simple metals. A key point emerging from this work is that the integrated surface charge-density perturbation $\int n dz$ is zero in the limit $q_{\parallel} \rightarrow 0$, in contrast to the regular surface plasmon which has a monopole or nonzero net charge, $\int n dz \neq 0$. An unequivocal prediction of multipole surface plasmons seems to require a microscopic theory in which the static density profile and the dynamic response can be made fully compatible (Dobson and Harris 1988).

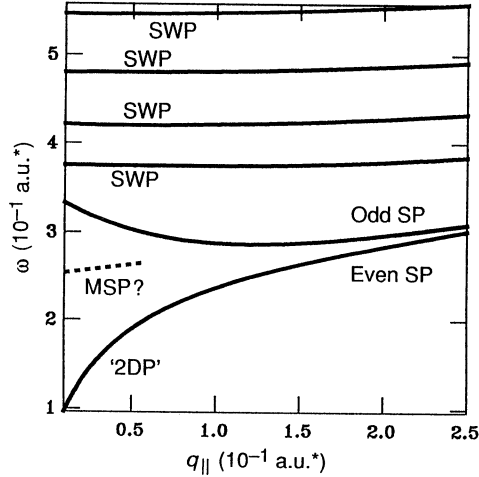


Fig. 8. Summary of the expected dispersion relations of collective plasmon excitations on a jellium slab of finite width, within a dispersive hydrodynamic approximation. Solid curves represent plasmons as predicted analytically using hard-wall boundary conditions [numerical solution of equations (9) and (10)]. The dashed line represents qualitatively the multipole surface mode expected when the hard-wall boundary condition is relaxed. SP denotes surface plasmons; 2DP, the mode with two-dimensional plasmon dispersion; SWP, bulk standing-wave plasmons; and MSP, multipole surface plasmons. Note that the standing-wave plasmon branches have an uneven spacing dependent on boundary conditions. (Solid curves were calculated for $r_s = 3$ and $L = 18$ to allow comparison with the microscopic WPQW calculation shown in Fig. 12.)

The above conclusions are summarised in Fig. 8, where the solid curves are the dispersion relations of the modes in the dispersive hard-wall approximation, as given by equations (9) and (10), with allowance for both real and imaginary values of Q . The dashed line represents a multipole surface plasmon whose

existence one might surmise from the smooth falloff of electron density at the edges of the well, as just discussed.

Other features of the excitation spectrum of quantum wells which plainly cannot be described in the hydrodynamic model include discrete-electron quantum effects such as resonances at single-particle transition energies, and other discrete-orbital and quantum size effects. Nevertheless the overall picture given in the above hydrodynamic model (Fig. 8) is a surprisingly good representation of the infrared spectrum of *wide* $\text{Ga}_{1-x}\text{Al}_x\text{As}$ quantum wells. Further progress, especially a reliable description of multipole surface plasmon and single-particle transition resonances, will require more microscopic models. These are established in the following two sections.

3. Kohn's Theorem: An Exact Result Specific to Parabolic Quantum Wells for $q_{\parallel} = 0$

The special case of an electron gas in a purely parabolic bare confining potential (WPQW) is unusual among quantum many-body systems in that an exact quantum mechanical result is available. In essence, the entire electron gas oscillates with a 'sloshing' motion in the z direction, at the same bare simple harmonic frequency $\omega_p = \sqrt{K/m}$ as applies for a single electron oscillating in the parabolic well. This holds for any central pair potential $u(|r|)$ acting between the electrons, and in particular it applies for the case in hand, that of the Coulomb pair potential. Note that ω_p is numerically equal to the 3D bulk plasma frequency for the positive background density n_0 corresponding to the given parabolic well (see the Introduction).

A formal proof of this 'Kohn (1961) theorem' result, which is the zero-magnetic-field case of a more general result given for parabolic wells including a static magnetic field by Brey *et al.* (1989), is as follows. For N particles labelled $\alpha = 1, \dots, N$ in a parabolic well, the total- z momentum and centre-of-mass operators $\hat{P}_z = \sum_{\alpha} \hat{p}_{z\alpha}$ and $\hat{Z} = \sum_{\alpha} \hat{z}_{\alpha}$ commute with the pair interaction. (The \hat{P}_z case amounts to conservation of total momentum when only central pair forces act between particles.) Then their commutators with the exact Hamiltonian are determined only by the kinetic energy part and the quadratic external-potential part $m\omega_p^2 \sum_{\alpha} z_{\alpha}^2/2$, giving

$$[\hat{H}_0, \hat{a}^{\pm}]_{-} = \pm \hbar\omega_p \hat{a}^{\pm}, \quad (13)$$

where

$$\hat{a}^{\pm} = m\omega_p \hat{Z} \pm i\hat{P}_z \quad (14)$$

are raising and lowering operators. Thus by standard operator algebra, as for a single simple harmonic oscillator, there exists a set of exact (many-body) eigenstates Ψ_n with energies spaced equally by $\hbar\omega_p$. Under a *spatially homogeneous* perturbing field $Ee^{-i\omega t}$ in the z direction, the perturbation is linear in $\sum_{\alpha} z_{\alpha}$, i.e. in $(\hat{a}^+ + \hat{a}^-)$, and thus couples states differing in energy by $\hbar\omega_p$, leading to a sharp absorption peak at ω_p .

While this generalised Kohn theorem only applies to resonance under a strictly uniform driving rf field, the physical nature of the electron gas motion in this

mode is a sloshing in the z direction across the parabolic well. Thus we expect, in the presence of a weakly nonuniform driving field of a grating-coupler WPQW experiment in the small- q_{\parallel} limit, to find a mode in which the sloshing is modulated in the x direction perpendicular to the electron gas surface (Fig. 6). If a transverse mode grades continuously into the uniform Kohn-theorem sloshing mode as $q_{\parallel} \rightarrow 0$, we expect that its frequency will approach ω_p in that limit. Such a mode does not compress the electron gas as $q_{\parallel} \rightarrow 0$, so that its finite frequency in this limit is not due to the electron-electron interaction, in contrast to the case of a bulk $q \rightarrow 0$ plasmon which also has frequency ω_p . Indeed, the Kohn-theorem mode of a jellium slab is a *transverse* plasmon, owing its finite frequency in the $q_{\parallel} \rightarrow 0$ limit to the parabolic confining potential. Later we will see from an explicit (but necessarily approximate) many-body calculation that the WPQW does indeed have a Kohn-theorem mode smoothly approaching ω_p as $q_{\parallel} \rightarrow 0$.

4. Approximate Microscopic Many-body Description of Quantum Well Plasmons

While the hydrodynamic treatment in Section 2 gives a rough guide to expected modes of oscillation, and a restricted exact result is available from Section 3 for a purely parabolic well, we need a detailed microscopic theory to cover all quantum wells of interest in a more reliable way.

The simplest such microscopic formalism is the time-dependent Hartree approach in which single electrons are treated quantum-mechanically, and are assumed to move in a mean-field potential determined self-consistently via Poisson's equation from the instantaneous electron density. Such an approach neglects exchange phenomena (due to the antisymmetry of many-electron wavefunctions under particle label transposition). It also neglects correlation phenomena (due to the tendency of individual Coulomb-interacting electrons to avoid one another, over and above the average repulsive effect inherent in the Hartree mean field). The simplest way to include exchange and correlation in inhomogeneous systems in general is the local density approximation (LDA) of Kohn and Sham (1965) (see Dreizler and Gross 1990).

(4a) Ground State of Electrons in a Quantum Well

The Kohn-Sham theory approximates exchange and correlation effects in inhomogeneous systems by using known results for the homogeneous electron gas. In its usual form it is a theory of the many-electron ground state. Applied to the ground state of a three-dimensional electron gas of area A in a bare quantum well potential $V(z)$ it gives the following equations (Dobson 1992) for effective one-electron eigenfunctions Ψ and electron number density $n(z)$:

$$\bar{\Psi}_{\mathbf{k}_{\parallel},j}(\mathbf{r}) = A^{-1/2} \exp(i\mathbf{k}_{\parallel} \cdot \mathbf{r}) \psi_j(z), \quad \mathbf{k}_{\parallel} = k_x \hat{x} + k_y \hat{y}, \quad (15)$$

$$\left(-\frac{\hbar^2}{2m} \frac{d^2}{dz^2} + V^{0\text{eff}}(z) \right) \psi_j(z) = \epsilon_j \psi_j(z), \quad \psi_j(z) \rightarrow 0 \text{ as } z \rightarrow \pm \infty, \quad (16)$$

$$n(z) = \sum_{\mathbf{k}_{\parallel},j \text{ occ}} |\bar{\Psi}_{\mathbf{k}_{\parallel},j}(\mathbf{r})|^2 = 2(2\pi)^{-2} \sum_{\epsilon_j < \epsilon_F} \pi(k_F^2 - 2m\epsilon_j/\hbar^2) \psi_j^2(z). \quad (17)$$

The self-consistent confining potential $V^{0\text{eff}}(z)$ is composed of the bare well potential $V^{\text{ext}}(z)$ plus a Hartree field and an exchange-correlation potential:

$$V^{0\text{eff}}(z) = V^{\text{ext}}(z) + V_{\text{H}}(z) + \mu_{\text{xc}}(z). \quad (18)$$

The Hartree (uncorrelated mean-field) potential satisfies the Poisson equation

$$(d^2/dz^2)V_{\text{H}}(z) = e^2 n(z)/\epsilon. \quad (19)$$

The exchange-correlation potential μ_{xc} is the only additional term which distinguishes the Kohn–Sham theory from the approximate Hartree theory. The exact nonlocal functional $\mu_{\text{xc}}[n]$ is, however, unknown. The LDA (Kohn and Sham 1965) consists of replacing this unknown functional by a local one:

$$\mu_{\text{xc}}(z) = \partial/\partial n(n\epsilon_{\text{xc}})|_{n=n(z)}. \quad (20)$$

Here the exchange and correlation energy ϵ_{xc} per electron of the uniform electron gas is reasonably well known for ‘metallic’ electron densities, by a variety of analytical and numerical methods (see e.g. Dreizler and Gross 1990). A very simple approximation, fairly accurate at metallic densities, is the Wigner interpolation formula (Mahan 1981, p. 397)

$$\epsilon_{\text{xc}} = -0.458/r_s - 0.44/(r_s + 7.8) \text{ a.u.}^*, \quad (21)$$

where $r_s = a_{\text{B}}^{* -1} (3n/4\pi)^{-1/3}$ is the inter-electron spacing in units of the Bohr radius.

The total number of electrons per unit area is

$$N_s = \int n(z) dz = (2\pi)^{-1} [k_{\text{F}}^2 N_{\text{occ}} - 2m\hbar^{-2}(\epsilon_1 + \epsilon_2 + \dots + \epsilon_{N_{\text{occ}}})]. \quad (22)$$

In the experimental situation (Fig. 2) the areal density N_s is controlled by (a) the amount of spatially remote doping, supplying free conduction band electrons to ‘fall’ into the well, and (b) the d.c. bias voltage maintained between the electron gas and the semi-transparent gate.

In solving the above Kohn–Sham equations for a given areal density N_s of electrons, the Fermi energy $\epsilon_{\text{F}} = \hbar^2 k_{\text{F}}^2/2m$ and the number N_{occ} of occupied 1D orbitals (‘sub-bands’) are determined self-consistently by increasing N_{occ} until the value of ϵ_{F} determined via (22) satisfies $\epsilon_{N_{\text{occ}}} < \epsilon_{\text{F}} < \epsilon_{N_{\text{occ}}+1}$.

Figs 4a and 4b show the total Kohn–Sham potential $V^{0\text{eff}}$ and ground-state electron density $n(z)$ resulting from a self-consistent solution of equations (15)–(22) for zero-temperature parabolic (WPQW) and neutral parabolic–linear (‘jellium slab’) wells. (See the Introduction for a discussion of these well structures: the bare external well potentials for these cases are shown in Fig. 1.) In both cases the electron gas lies in a fairly uniform layer of density equal to that of the fictitious epitaxially grown effective positive background, and $V^{0\text{eff}}$ is almost uniform inside the layer. The differences between the two types of well are found at the edges. In the jellium slab case the correctly filled well plus effective positive background constitute an electrically neutral system, and accordingly

the total effective potential $V^{0\text{eff}}(z)$ levels off outside the electron gas, giving rise to a well-defined work function $V^{0\text{eff}}(z \rightarrow \infty) - \epsilon_F$. The electron density has considerable penetration into the vacuum. In the WPQW case we effectively have a system which is not electrically neutral, since the positive background extends outside the layer of electron gas. The potential $V^{0\text{eff}}$ rises quadratically outside the well, forcing the electron gas density to fall rather abruptly at its edges. These sharp edges have been termed (Dobson 1992) ‘embedded’ electron gas edges, and they constitute a new type of surface physics problem distinct from the standard jellium edge situation described theoretically by Lang and Kohn (1970). The contrast between the ‘regular’ or Lang–Kohn electron gas edge density and that of the ‘embedded’ electron gas edge is highlighted in Fig. 9 using a suitable scale. We will see shortly that the dynamic properties of the embedded electron gas edge are correspondingly different from those of regular jellium (Dobson 1992; Pinsukanjana *et al.* 1992).

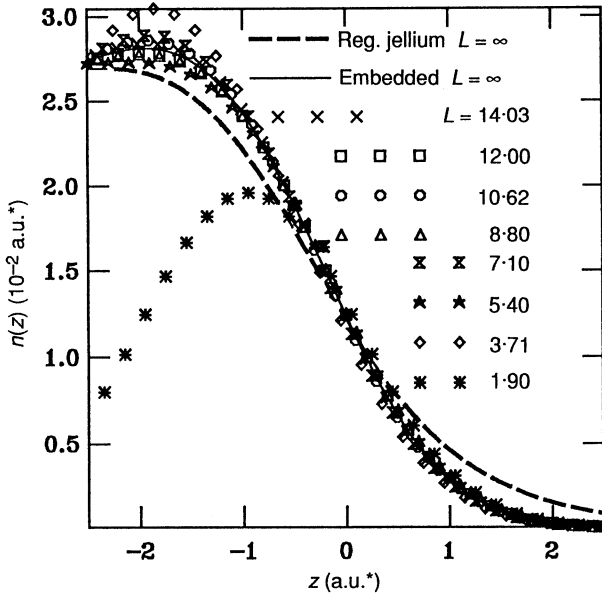


Fig. 9. Details of the static electron density distribution near the edge (set here to $z = 0$) of the electron gas layer in a WPQW, showing its stability as a function of electron gas layer thickness L (symbols), with $r_s^* = 2.07$. The thin curve (visible only near the top of the figure) is the case $L \rightarrow \infty$. All the above results show a sharper edge profile than a regular jellium surface (dashed curve). [From Dobson (1992).]

(4b) Bare Response of Quantum Well Electrons to Time-varying External Fields

To linear order, the density response of an interacting zero-temperature many-electron system to a *static* external potential $\delta V^{\text{ext}}(r)$ can be derived without further approximation from the Kohn–Sham equations (see e.g. Dobson and Rose 1982, Appendix A2). The method stems from the fact that the Kohn–Sham

density is formally that of independent electrons moving in an effective field. The density response $\delta n(\mathbf{r})$ of such independent electrons to a change $\delta V^{\text{eff}}(\mathbf{r}')$ in the effective potential can be found straightforwardly by adding the squared moduli of one-electron wavefunctions augmented with a standard first-order perturbation correction. The result is, in general geometry,

$$\delta n(\mathbf{r}) = \int d\mathbf{r}' \chi_0(\mathbf{r}, \mathbf{r}') \delta V^{\text{eff}}(\mathbf{r}') \equiv \chi_0 * \delta V^{\text{eff}}, \quad (23)$$

where the asterisk represents spatial convolution and the bare (generalised Lindhard or single-bubble) susceptibility is

$$\chi_0(\mathbf{r}, \mathbf{r}', \omega) = 2 \sum_{I,J} \frac{f_I - f_J}{E_I - E_J - \hbar\omega - i0} \Psi_I^*(\mathbf{r}) \Psi_J^*(\mathbf{r}') \Psi_J(\mathbf{r}) \Psi_I(\mathbf{r}'). \quad (24)$$

We have included a finite frequency ω from standard time-dependent perturbation theory even though so far we are only justified in using the $\omega \rightarrow 0$ limit. In (24) $\{E_I\}$ are the unperturbed Kohn–Sham eigenenergies, which for the slab geometry of interest here are

$$E_J \equiv E(\mathbf{k}_{\parallel}, j) = \hbar^2 k_{\parallel}^2 / 2m + \epsilon_j \quad (25)$$

and f_J is, in the present case, the zero-temperature Fermi distribution. Note that for a uniform electron gas the space Fourier transform $\chi_0(q, \omega)$ of (24) is the standard Lindhard response containing logarithmic singularities (Mahan 1981). Using (25) in (24) we find

$$\chi_0(\mathbf{r}, \mathbf{r}', \omega) = (2\pi)^{-2} \int d^2 q_{\parallel} \exp(i\mathbf{q}_{\parallel} \cdot \mathbf{r}) \chi_0(q_{\parallel}, z, z', \omega), \quad (26)$$

where

$$\begin{aligned} \chi_0(q_{\parallel}, z, z', \omega) &= 2 \sum_{i,j} (2\pi)^{-2} \int d^2 k_{\parallel} f(\epsilon_i + \hbar^2 k_{\parallel}^2 / 2m) \psi_i(z) \psi_i(z') \psi_j(z) \psi_j(z') \\ &\times \{[\epsilon_i - \epsilon_j + \hbar\omega + \hbar^2(2k_x q_{\parallel} - q_{\parallel}^2) / 2m]^{-1} \\ &+ [\epsilon_i - \epsilon_j - \hbar\omega - \hbar^2(2k_x q_{\parallel} + q_{\parallel}^2) / 2m]^{-1}\}. \end{aligned} \quad (27)$$

The dummy labels i and j have been interchanged in obtaining the second term in braces.

(4c) Screening the Bare Response

In Section 4b the density response to a change δV^{eff} , rather than to a change δV^{ext} , was obtained. The change δV^{eff} in the total effective potential must now be related to the externally imposed perturbation δV^{ext} by linearising the self-consistency conditions (18)–(20). There results a spatial integral equation (the ‘screening’ equation) which in convolution notation can be abbreviated as

$$\delta n = \chi_0 * (\delta V^{\text{ext}} + V_c * \delta n + f_{\text{xc}} \delta n). \quad (28)$$

Here, for the static case,

$$f_{xc}(\mathbf{r}) = (\partial^2/\partial n^2)[n\epsilon_{xc}(n)]_{n=n(\mathbf{r})}. \quad (29)$$

The case of time-dependent perturbations requires further assumptions since the standard Kohn–Sham approach is a ground-state theory. Nevertheless, it is now commonplace (Ando 1977; Zangwill and Soven 1980; Dobson and Harris 1986; Tsuei *et al.* 1991) to use equations (24), (28) and (29) at finite frequency, unmodified. The resulting scheme is widely known as the time-dependent local density approximation (TDLDA). Although a general density functional approach to time-dependent phenomena is difficult, Gross and Kohn (1985) and Iwamoto and Gross (1987) have proposed a tractable scheme for the special case of linear response. In their scheme, which we term the dynamic local density approximation (DLDA), f_{xc} in equation (29) is replaced by $f_{xc}(n(r), \omega)$ where the ω dependence is determined by an analytic interpolation between the static limit (29) and the high-frequency limit determined from frequency moment sum rules. Results from the DLDA are not very different from those of the TDLDA for the low- r_s jellium surface (Dobson and Harris 1990), but the differences are expected to be greater at higher r_s .

Both the TDLDA and DLDA discussed above have a *local* exchange-correlation term, but since the screening equation (28) already involves convolutions it is not difficult to allow for a nonlocal but linearised xc term:

$$\delta n = \chi_0 * (\delta V^{\text{ext}} + V_c * \delta n + F_{xc} * \delta n), \quad (30)$$

where both χ_0 and F_{xc} can depend on q_{\parallel} , z , z' and ω . Of course, it will only be valid to use a nonlocal linearised xc term F_{xc} in (30) if the ground-state equation (20) is also made nonlocal and consistent with f_{xc} in the static limit.

5. Proof of Existence of a Mode with 2D Plasmon Dispersion as $q_{\parallel} \rightarrow 0$

We now show that the bare response formula (27) and the generalised screening equation (30) imply the existence, for an arbitrary bare confining potential $V^{\text{ext}}(z)$ acting on 3D electrons, of a plasmon mode with dispersion

$$\omega^2 \underset{q_{\parallel} \rightarrow 0}{\approx} N_s e^2 q_{\parallel} / 2\epsilon m. \quad (31)$$

The only restrictions on this result are as follows:

(a) The background dielectric constant ϵ and effective mass m are assumed to be position-independent.

(b) The wavevector must be small: specifically, $q_{\parallel} W \ll 1$, $q_{\parallel} v_0 \ll \omega_{2D}$. Here W is the distance, in the z direction, between the outermost limits of the electron charge distribution (both the static and dynamic parts), while v_0 is a mean electron velocity, v_F at low T or v_{thermal} at high T .

(c) We must have precisely slab geometry—electrons are free to move in the x and y directions and are confined by a potential $V(z)$ independent of x and y .

(d) The exchange-correlation kernel F_{xc} must be less singular than q_{\parallel}^{-1} as $q_{\parallel} \rightarrow 0$ (this is certainly true of any local form because F_{xc} is then independent of q_{\parallel}).

Note that, although the dispersion law (30) is as for a 2D electron gas, the electron gas does *not* have to be thin: condition (b) merely requires a small surface-parallel wavevector. In fact the theorem holds even for multiple well structures, in which case W in condition (b) above is approximately the entire width of the multi-well structure. It also holds for any temperature (though note that the width W as defined above will increase with temperature). It furthermore holds for all local and many nonlocal xc expressions.

To establish the theorem, we investigate the solutions of (30) in the limit of a small surface-parallel wavevector q_{\parallel} , for finite ω . To this end we first expand the braces in (27) to third order in the small quantities $(\hbar^2/2m)(2k_x q_{\parallel} \pm q_{\parallel}^2)/\hbar\omega$. After integrating over z , using orthonormality of the $\{\psi_i(z)\}$ we obtain

$$\int \chi^0(\omega, q_{\parallel}, z, z') dz' = \frac{q_{\parallel}^2}{\omega^2 m} n^0(z) + \frac{6q_{\parallel}^4}{m^2 \omega^4} t_x^0(z) + O(q_{\parallel}^6/\omega^4) \quad (32a)$$

$$= \int \chi^0(\omega, q_{\parallel}, z', z) dz', \quad (32b)$$

where

$$n^0(z) = \sum_i \frac{2}{(2\pi)^2} \int d^2 k_{\parallel} f\left(\epsilon_i + \frac{\hbar^2}{2m} k_{\parallel}^2\right) |\varphi_i(z)|^2 \quad (33)$$

is the static zeroth-order density profile and

$$t_x^0(z) = \sum_i \frac{2}{(2\pi)^2} \int d^2 k_{\parallel} f\left(\epsilon_i + \frac{\hbar^2}{2m} k_{\parallel}^2\right) |\varphi_i(z)|^2 \frac{\hbar^2}{2m} k_x^2 \quad (34)$$

is the density of kinetic energy of the x -motion (parallel to q_{\parallel}) in the static problem. Equation (32b) is identical to (32a) except that z and z' have been interchanged inside χ^0 (reciprocity). Similar results have been used previously (Harris and Griffin 1971; Feibelman 1971) to prove that the surface plasmon mode on metallic surfaces approaches a frequency $\omega_p/\sqrt{2}$ in the long-wavelength limit.

[At finite temperature the energy denominators in (27) for small q_{\parallel} can always vanish at sufficiently large k_x of order $m\omega/\hbar q_{\parallel}$, formally invalidating the above expansion. However, the corresponding Landau damping terms are down by a factor $\exp(-m\omega^2/q_{\parallel}^2 k_B T)$ because of the thermal distribution f appearing in (27), and are hence negligible in solid state applications. In the present case of the '2D plasmon mode', ω^2 is proportional to q_{\parallel} , leaving a very small $\exp(-\text{const.}/q_{\parallel})$ factor in the neglected terms.]

The screening equation (30) can be written, with the most general form of xc kernel,

$$\begin{aligned} \delta n(z) - \int dz' dz'' \chi^0(\omega, q_{\parallel}, z, z') \left(\frac{2\pi e^2}{q_{\parallel}} e^{-q_{\parallel}|z'-z''|} + F_{xc}(\omega, q_{\parallel}, z', z'') \right) \delta n(z'') \\ = \int \chi^0(\omega, q_{\parallel}, z, z') \delta V^{\text{ext}}(z') dz'. \end{aligned} \quad (35)$$

In the DLDA (Gross and Kohn 1985), for example

$$F(\omega, q_{\parallel}, z', z'') = \delta(z' - z'') f_{xc}(\omega, n^0(z')) \quad \text{for all } q_{\parallel}, \quad (36)$$

with f_{xc} replaced by its zero-frequency value $(\partial\mu_{xc}/\partial n)|_{n^0(r)}$ in the case of the more usual TDLDA.

In equation (35) we allow in fact for a more general, nonlocal exchange and correlation kernel $F_{xc}(\omega, z, z')$: to obtain (31) we need to assume that it is less singular as $q_{\parallel} \rightarrow 0$ than the bare Coulomb kernel $2\pi e^2 q_{\parallel}^{-1} \exp(-q_{\parallel} |z - z'|)$. The plasmon modes are the homogeneous solutions of equation (35), i.e. those self-sustaining oscillatory solutions for which $\delta V^{\text{ext}}(z) = 0$. We break up the Coulomb kernel as follows:

$$e^2 q_{\parallel}^{-1} e^{-q_{\parallel} |z|} / 2\epsilon = e^2 \left(q_{\parallel}^{-1} + \frac{e^{-q_{\parallel} |z|} - 1}{q_{\parallel}} \right) / 2\epsilon, \quad (37)$$

where the second term approaches the finite limit $-e^2 |z| / 2\epsilon$ as $q_{\parallel} \rightarrow 0$.

Using the decomposition (37) we integrate (35) with respect to z , putting $\delta V^{\text{ext}} = 0$ as appropriate for free plasmon oscillations. Then using the identity (32) and writing

$$\int \delta n(z) dz = M_0, \quad (38)$$

we obtain the dispersion relation

$$\begin{aligned} M_0 - \left(\frac{q_{\parallel}}{\omega^2 m} N_s^0 + \frac{6q_{\parallel}^4}{\omega^4 m^2} T_x^0 N_s^0 + O(q_{\parallel}^6/\omega^6) \right) \frac{2\pi e^2}{q_{\parallel}} M_0 \\ + \left(\frac{q_{\parallel}^2}{\omega^2 m} + O(q_{\parallel}^4/\omega^2) \right) \int dz' dz'' n^0(z') \\ \times \left(\frac{2\pi e^2}{q_{\parallel}} (e^{-q_{\parallel} |z' - z''|} - 1) + F_{xc}(\omega, q_{\parallel}, z', z'') \right) \delta n(z'') = 0. \end{aligned} \quad (39)$$

Here $N_s = \int n^0(z) dz$ is the static areal electron density and

$$\begin{aligned} T_x^0 &= \int t_x^0(z) dz / N_s^0 \\ &= \frac{\hbar^2}{2m} \sum_i \int_0^{\infty} \frac{1}{2} k^3 f \left(\epsilon_i + \frac{\hbar^2}{2m} k^2 \right) dk / \sum_i \int_0^{\infty} k f \left(\epsilon_i + \frac{\hbar^2}{2m} k^2 \right) dk \end{aligned} \quad (40)$$

is the equilibrium kinetic energy, per electron, of motion parallel to \mathbf{q}_{\parallel} .

Letting $q_{\parallel} \rightarrow 0$ and keeping only the $O(1)$ and $O(q_{\parallel})$ terms in (39) we recover the well-known lowest-order 2D plasmon dispersion relation $\omega^2 = e^2 N_s m^{-1} q_{\parallel} / 2\epsilon$, where we have assumed that $M_0 \neq 0$ so that M_0 can be cancelled throughout. Taking this value of ω in the higher terms and multiplying (39) throughout by

ω^2/M_0 we obtain a formal expression for the leading $q_{\parallel} \rightarrow 0$ corrections to the ‘2D plasmon’ dispersion of an arbitrarily thick slab:

$$\omega^2 = e^2 N_s m^{-1} q_{\parallel} / 2e + m^{-1} (6T_x^0 - U^0) q_{\parallel}^2 + O(q_{\parallel}^3). \quad (41)$$

Here

$$U^0 = \int dz' dz'' n^0(z') [e^2 |z' - z''| / 2\epsilon - F_{xc}(\omega_{2D}(q_{\parallel}), q_{\parallel} \rightarrow 0, z', z'')] \delta n(z'') \bigg/ \int \delta n(z) dz \quad (42)$$

is the positive energy of Coulomb repulsion per electron in the $q_{\parallel} \rightarrow 0$ limit, averaged between the equilibrium density and the plasmon mode profile $\delta n(z)$ (which solves equation 35). This is well-defined provided that the exchange-correlation kernel F_{xc} remains finite as $q_{\parallel} \rightarrow 0$. This is certainly the case for local approximations to F_{xc} , such as the TDLDA or DLDA, but one can deduce indirectly that it cannot be the case if F_{xc} is sufficiently nonlocal to change the effective mass: in that case the U^0 term above must presumably be singular enough to compete with the leading dispersion term $\omega^2 = N_s e^2 q_{\parallel} / 2\epsilon m$, in such a way as to change the effective value of m .

For the case of a sufficiently wide well the $|z - z'|$ term in (42) is dominant over the other term in (42) and also over the T_x^0 term in (41). If we introduce a maximum width W of the density distributions $n(z)$ and $\delta n(z)$, then the modulus of U^0 is bounded as follows:

$$|U^0| < a W N_s / \epsilon, \quad (43)$$

where N_s is the ground-state areal density and

$$a = \int |\delta n(z)| dz \bigg/ \left| \int \delta n(z) dz \right| \quad (44)$$

is a number of order 1 for the case at hand in which the denominator of (44) is finite. [Strictly speaking it is necessary to assume that a does not diverge as $q_{\parallel} \rightarrow 0$, which amounts to assuming that $\delta n(z)$ has a stable limit as $q_{\parallel} \rightarrow 0$: this is borne out by numerical calculations.]

Using (43) in (41) we find, for wide wells,

$$\omega^2 = e^2 N_s m^{-1} q_{\parallel} (2\epsilon)^{-1} [1 + O(W q_{\parallel})]. \quad (45)$$

Thus, even for wide wells, the ‘2D’ plasmon dispersion law holds.

The above derivation assumes that we are dealing with a mode for which $\delta n(z)$ remains finite and has a nonzero integral $M_0 = \int \delta n(z) dz$ in the limit $q_{\parallel} \rightarrow 0$. There are other modes such as the ‘centre of mass’ or sloshing mode of a wide parabolic quantum well (or ‘interband’ modes in general), plus in some cases other ‘intraband’ modes (Fasol *et al.* 1989) which do not have this property and correspondingly have quite a different low- q_{\parallel} dispersion.

There are other ways (Kempa *et al.* 1989; Das Sarma 1992, personal communication) of obtaining a 2D plasmon-like dispersion on a general well,

but the present approach has the advantage of including exchange-correlation, quantifying the next term and obtaining a simple physical criterion for the region of validity.

6. Formulae for Numerical Quantum Well Response Calculations

(6a) Discrete Basis Methods

The expression (24) for the bare response, while written in real (z, z') space, employs an infinite sum over the 1D eigenfunctions for motion across the well. Some numerical work has used this infinite discrete eigenfunction expansion, coupled with a Fourier series (k_z, k_z') representation in the z direction (Eguiluz 1983; Kempa *et al.* 1989).

Another variant is exemplified by Das Sarma (1984): he used a fully matrix-element oriented description, which can be derived by decomposing the density response into components

$$\delta\rho_{mn}(t) = \{ \langle c_m^\dagger c_n \rangle_t - \langle c_m^\dagger c_n \rangle_{\text{equil}} \} + \{ \text{complex conjugate} \}, \quad (46)$$

representing the density perturbation due to a small amount of the sub-band n becoming mixed into the sub-band m by the time-dependent potential. The bare response of $\delta\rho_{mn}$ has peaks at the single-particle ('sub-band') energy eigenvalue difference $\epsilon_m - \epsilon_n$. The screening equation (30) becomes a matrix equation and the condition for free plasmon oscillations can be written, within the time-dependent Hartree (RPA) approximation (Das Sarma 1984), as

$$0 = \det\{\epsilon_{ijmn}(q_{\parallel}, \omega)\} = \det\{\delta_{im} \delta_{jn} - v_{ijmn} \chi_{mn}^0\}. \quad (47)$$

This is an $N^2 \times N^2$ problem, where N is the number of sub-bands kept: for exact results, of course, we must let $N \rightarrow \infty$. For only one or two sub-bands occupied, and with unevenly spaced energy levels, equation (47) can be reasonably approximated by a 4×4 system ($N = 2$), however. Das Sarma (1984) has shown that this approach gives essentially analytic results for 'intra-sub-band' (2D plasmon) and 'inter-sub-band' plasmons in the case of heterojunctions with only one occupied sub-band: this version of the formalism clearly has great advantages in this limit. Here, however, we are interested in wider wells for which N must be increased, making the $N^2 \times N^2$ nature of the eigenproblem increasingly unwieldy. A real-space approach is more suitable for elucidating the surface nature of the plasmon modes in wider parabolic and related wells, and we outline this next.

(6b) Real-space (z, z') Approach

Another form suitable for numerics can be obtained by noting (Feibelman 1982) that the sum over 1D eigenstates ψ_j in (27) is the Green function for a 1D Schrödinger equation. This Green function can also be represented as a product of left and right eigenfunctions ψ^L, ψ^R with an appropriate derivative discontinuity at $z = z'$. Then, after some algebra, (27) becomes

$$\begin{aligned} \chi_0(q_{\parallel}, z, z', \omega) &= -2m(\pi^2\hbar^2)^{-1} \sum_{i \text{ occ}} \psi_i(z) \psi_i(z') \int_{-k_i}^{k_i} dk_x (k_i^2 - k_x^2)^{1/2} \\ &\times [\{\psi^{\text{R}}(\epsilon^+, z_{>}) \psi^{\text{L}}(\epsilon^+, z_{<}) / [W(\psi^{\text{R}}(\epsilon^+), \psi^{\text{L}}(\epsilon^+))] \} + \{\epsilon^+ \rightarrow \epsilon^-\}]. \end{aligned} \quad (48)$$

Here

$$\epsilon^{\pm} = \pm \hbar\omega + \epsilon_i + \hbar^2(\pm 2k_x q_{\parallel} - q_{\parallel}^2)/2m, \quad (49)$$

$$k_i^2 = 2m\hbar^{-2}(\omega_{\text{F}} - \epsilon_i), \quad z_{>} = \max(z, z') \text{ and } z_{<} = \min(z, z').$$

In (48), ψ^{R} and ψ^{L} are homogeneous solutions of equation (16) satisfying zero boundary conditions at $z \rightarrow +\infty$ and $z \rightarrow -\infty$ respectively. The Wronskian

$$W = \psi^{\text{R}} \partial \psi^{\text{L}} / \partial z - \psi^{\text{L}} \partial \psi^{\text{R}} / \partial z \quad (50)$$

of the left and right solutions can be shown to be z -independent because both ψ^{R} and ψ^{L} satisfy (16) at the same (complex) energy.

Equation (48) avoids the infinite sum over intermediate states j inherent in (24), but instead the left and right wavefunctions $\psi^{\text{L}}, \psi^{\text{R}}$ are obtained numerically at each k_x value sampled in the numerical k_x integration. For small finite values of q_{\parallel} , (48) is considerably more efficient than (24) for calculation of χ_0 because, as shown by (49), the argument of $\psi^{\text{L}}, \psi^{\text{R}}$ hardly varies and the k_x integration can be done with a handful of points. The square root in the k_x integral is handled by a purpose-built algorithm so that fine sampling is not required.

7. Numerical Results for Parabolic and Related Wells under Grating Coupler Excitation

The response of parabolic wells at $q_{\parallel} = 0$ is relatively uninteresting because of the generalised Kohn theorem (see Section 3) and because external fields with $q_{\parallel} \approx 0$ have the wrong z -dependence and hence cannot excite standing plasmon waves with discrete wavenumber across the well (see Section 2c). More interesting behaviour occurs if we excite the well at finite q_{\parallel} using a grating coupler (see Fig. 2). While a more detailed theory has been given for the strong coupling of a grating to a nearby two-dimensional system (Zheng *et al.* 1990; Zheng and Schaich 1991; Schaich 1992, personal communication), we consider here only the case of weak coupling between the grating and the electron gas. This case may be understood by introducing the grating strength parameters $\beta_n(\omega)$ defined as follows. Consider an r.f. field incident normally on the grating. In the absence of the electron gas it produces a $q_{\parallel} = 0$ electric field component at the grating position z_{g} given by $E_0 \hat{x} \exp(-i\omega t)$. The grating then produces a near field with components at surface-parallel wavevectors $\mathbf{q}_{\parallel} = \mathbf{q}_n = (2\pi n/\lambda_g) \hat{x}$. Because this field has $\nabla \times \mathbf{E} \approx 0$ in the nonretarded limit, it may be represented as the gradient of a near potential ϕ :

$$\phi(r) = E_0 \sum_{n=1}^{\infty} \beta_n(\omega) \exp(-q_n |z - z_{\text{g}}| + iq_n x - i\omega t). \quad (51)$$

Note that this potential has $\nabla^2 \phi = 0$ for $z \neq z_{\text{g}}$, and that the higher components fall off more rapidly away from the grating than do the low ones $n = 1, 2, \dots$. Note

also that β_n could depend on E_0 (i.e. the grating could respond nonlinearly), but we assume here that the incident and returned fields are weak enough that the nonlinearity can be neglected. Using the screening equation (28), (35) we calculate numerically the linear density response $\delta n(z) \exp(iq_{\parallel} x - i\omega t)$ of the confined electrons in the well to this potential:

$$\delta n(\mathbf{r}, t) = -eE_0 \sum_{n=1}^{\infty} \beta_n(\omega) \delta n^{(n)}(z) \exp(-q_n z_g + q_n x - i\omega t). \quad (52)$$

Here $\delta n^{(n)} \exp(iq_n x - i\omega t)$ is the response from the screening equation (28), (35) to a single component n of the grating field, of unit strength: that is, it is the response to a potential $\phi = \exp(q_n z + iq_n x - i\omega t)$. We have assumed that the grating lies outside the electron gas and to the right, so that in the perturbing potential we may write $\exp(-q_n |z - z_g|) = \exp(q_n z) \exp(-q_n z_g)$.

Using $E = -\nabla\phi$ and integration by parts, we calculate the power absorbed per unit area of well:

$$\begin{aligned} P &= A^{-1} \text{Re} \int J^* E^{\text{ext}} d^3r \\ &= \omega e^2 E_0^2 \sum_n |\beta_n(\omega)|^2 \exp(-2q_n z_g) \text{Im}\{M(q_n, \omega + i0)\}. \end{aligned} \quad (53)$$

Here M is an exponential moment of the density response,

$$\begin{aligned} M(q_{\parallel}, \omega) &= \int \delta n(z) \exp(q_{\parallel} z) dz \\ &= \int \exp(q_{\parallel} z') \chi(q_{\parallel}, \omega, z, z') \exp(q_{\parallel} z) dz dz', \end{aligned} \quad (54)$$

where $\delta n(z)$ is the solution to the screening integral equation (35) with $\delta V^{\text{ext}}(z) = \exp(q_{\parallel} z)$ and χ is the *screened* susceptibility. In (53) the cross terms involving $n \neq n'$ vanish because the surface integral of $A^{-1} \exp\{(q_n - q_{n'})x\}$ vanishes for $n \neq n'$ in the limit of large surface area A .

The above method takes into account the effect of the grating in adding surface-parallel momenta, $\Delta q_{\parallel} = q_n$ ($n \neq 0$). In order to obtain realistic experimental absorption predictions for the '2D plasmon' line by this method, one should also take into account the $\Delta q_{\parallel} = 0$ effect of the grating and gate: in a first approximation these act as a grounded conducting plane for the self-consistent fields of the confined electrons. Thus, the Coulomb kernel in the screening equation (35) should be replaced as follows:

$$e^2 \exp(-q_{\parallel} |z - z'|) \rightarrow e^2 \exp(-q_{\parallel} |z - z'|) - e^2 \exp(-q_{\parallel} |2z - z_0|).$$

[In a more complete theory of strongly-coupled gratings (Zheng *et al.* 1990; Zheng and Schaich 1991; Schaich 1992, personal communication) the $\Delta q_{\parallel} = 0$ and the $\Delta q_{\parallel} \neq 0$ effects of the grating and gate are treated on an equal footing.]

To obtain the numerical results shown below, the bare susceptibility χ_0 (equation 48) was evaluated on a discrete grid of z, z' points for frequencies

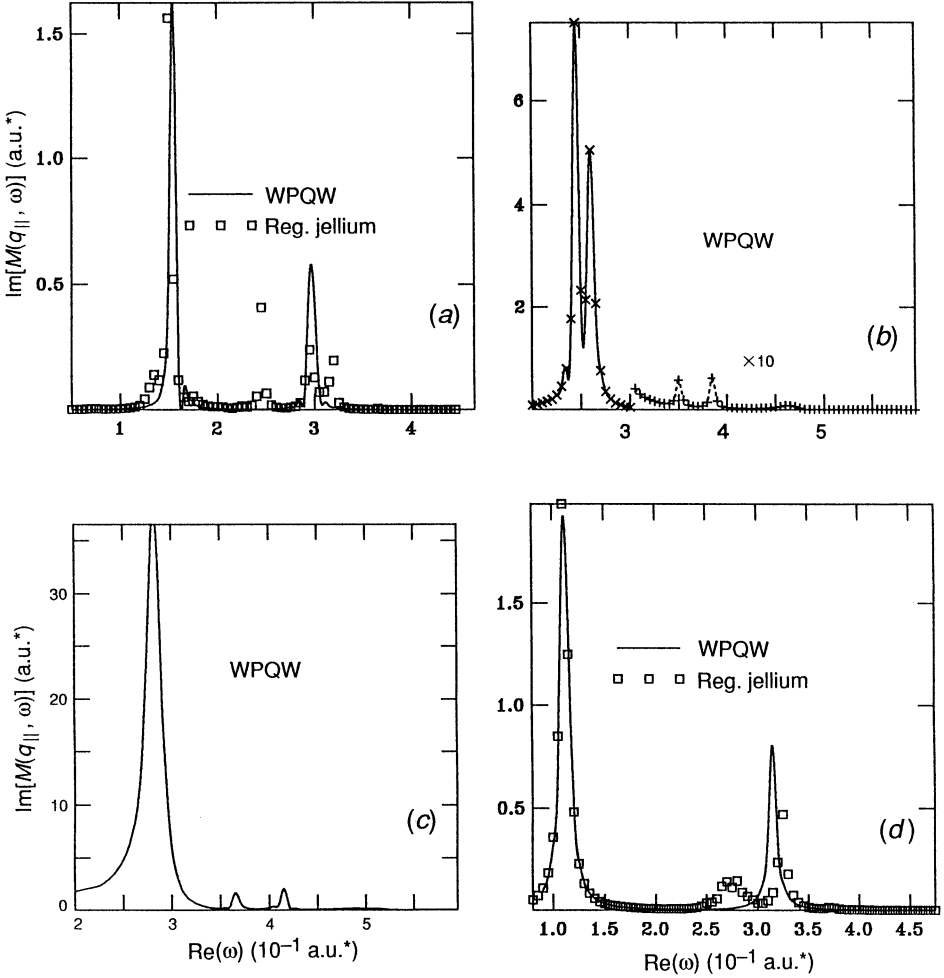


Fig. 10. Spectral absorption function $-\text{Im}[M(q_{\parallel}, \omega)]$ from equation (54) for $\tau_s^* = 3$, with an arbitrarily chosen imaginary frequency component $\text{Im}(\omega) = 0.002$ a.u.*:

(a) Spectra for electron gas layer 18 a.u.* wide with a low surface wavenumber $q_{\parallel} = 0.03$ a.u.* , showing the presence of the multipole surface mode (middle peak, squares) for a linear-parabolic well representing regular jellium. The surface multipole is absent for the WPQW (solid curve).

(b) Spectrum for a WPQW with $L = 18$ a.u.* and a larger surface wavenumber $q_{\parallel} = 0.15$ a.u.* . The two main peaks are beginning to coalesce into a single surface plasmon frequency, and standing-wave plasmons (with vertical scale amplified by 10) are starting to strengthen.

(c) Spectrum for a WPQW with $L = 18$ and a large surface wavenumber $q_{\parallel} = 0.25$. Only a single surface plasmon peak can now be resolved, and there are two standing-wave plasmons with a hint of a third.

(d) Spectra for a WPQW (solid curve) and for a neutral jellium (linear-parabolic) well containing a wider electron gas, $L = 25$ a.u.* , and a low surface wavenumber. The multipole surface plasmon between the two main peaks is still visible on the regular jellium slab and absent on the WPQW.

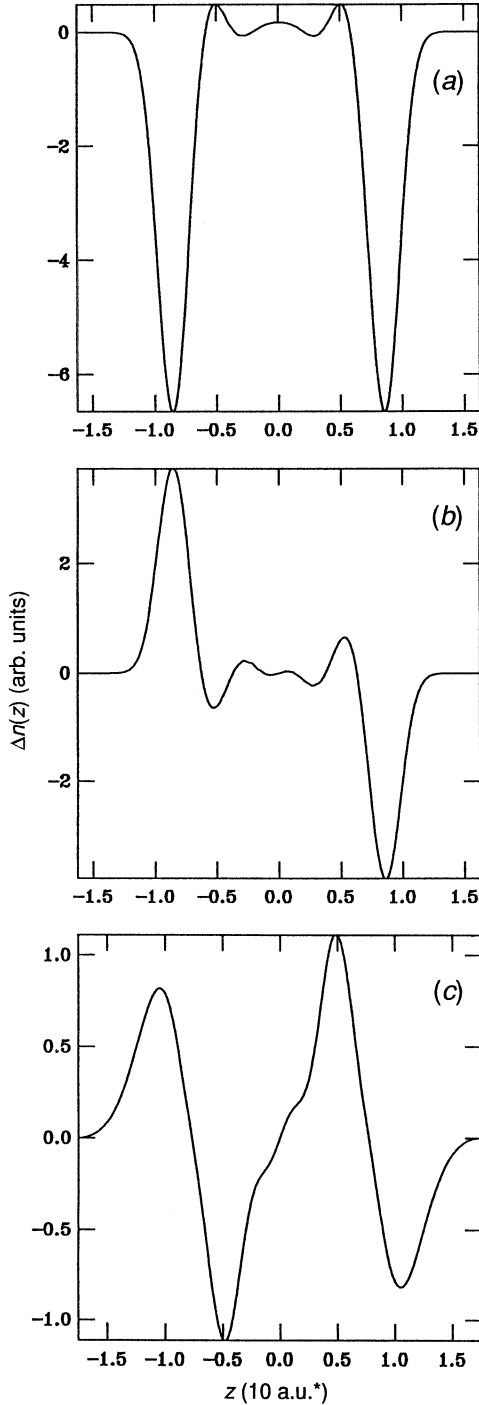


Fig. 11. Calculated mode profiles $\Delta n(z)$ (spatial distribution of oscillatory electron charge density perturbation) for $r_s = 3$, $L = 18$ and $q_{\parallel} = 0.01$: (a) Mode with '2D plasmon' dispersion, showing that despite its dispersion it is an even combination of two surface charge perturbations. (For very thin electron layers these perturbations coalesce to form a true 2D plasmon.) (b) Centre-of-mass, Kohn-theorem or 'sloshing' mode, showing out-of-phase disturbances at the two surfaces. (c) Multipole surface plasmon on a neutral jellium slab. Each half of the slab is approximately charge neutral. [From Dobson (1992).]

$\omega_R + i\omega_I$ lying just above the real axis (ω_I was arbitrarily chosen as 0.002 a.u.*). The Wronskian (50) has zeros whenever $\epsilon_{\pm} = \epsilon_j$ (see equation 49) for any well eigenstate j . These zeros correspond to the unshifted single-particle resonances in the discrete-summation approaches mentioned above, and they are smeared by the k_x integration for finite q_{\parallel} . These singularities in (48) were treated numerically by adding and subtracting an analytically-integrable expression with the same poles and residues, leaving a smooth function to be numerically integrated, plus an analytic correction term. The 1D screening integral equation (35) (with local static Wigner xc) was discretised on the same discrete set of z points, using appropriate weights to convert z integration to summation taking into account the cusps at $z = z'$ in χ_0 and in the Coulomb kernel. The density response $\delta n(z) = \int \chi \exp(q_{\parallel} |z - z'|) dz'$ was thus found as the solution of N linear equations, where N is the number of discrete z points, which ranged up to 149. For each value of ω and each q_{\parallel} , the absorption function $M(q_{\parallel}, \omega)$ from equation (54) was then computed by one further 1D numerical integration. Some typical results are shown in Figs 10, 11 and 12 for pure parabolic wells and also for linear-parabolic quantum wells filled to neutrality. Some further cases can be found in Dobson (1992).

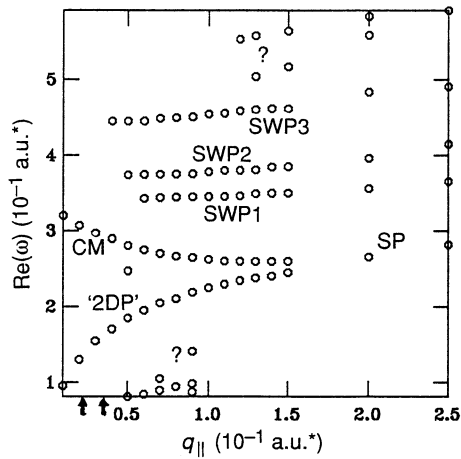


Fig. 12. TDLDA dispersion relations on a WPQW for $r_s^* = 3$ and $L^* = 18$. The 2D-plasmon-like mode (2DP) and the centre-of-mass mode (CM) clearly coalesce at high q_{\parallel} to form the surface plasmon (SP). Three standing-wave plasmons (SWP1, SWP2, SWP3) are also apparent at high q_{\parallel} . The weak low frequency modes marked '?' may be related to the intraband modes of Fasol *et al.* (1989). The high-frequency modes marked '?' may be higher standing-wave plasmons. The general similarity to Fig. 8 is striking.

Consider first the pure parabolic wells (WPQWs). The IR absorption function $-\text{Im}[M(q_{\parallel}, \omega)]$ at low q_{\parallel} (curves in Figs 3*b*, 10*a* and 10*d*) shows only two significant peaks. One is at the 2D plasmon frequency (equation 45) predicted by the theorem of Section 5, and one is close to the Kohn-theorem frequency ω_p . This is in good agreement with the experimental data of Pinsukanjana *et al.* (1992)

(Fig. 3a). The dominance of the 2D plasmon peak at low q_{\parallel} can be understood from its mode profile $\Delta n(z)$ (Fig. 11a) which has a nonzero moment $\int \Delta n(z) dz$. It therefore couples to the grating's near-field potential [which is proportional to $\exp(q_{\parallel} z) \approx 1 + q_{\parallel} z \dots$] even in the limit $q_{\parallel} \rightarrow 0$. The Kohn-theorem or sloshing mode has an odd profile (Fig. 11b) and so only couples to $O(q_{\parallel})$. As q_{\parallel} is increased (Figs 10b and 10c) some peaks above ω_p gain strength. These appear to be standing plasmons with oscillatory mode profiles, explaining their weak coupling at low q_{\parallel} . Unfortunately, for $r_s^* = 2.07$ and $q_{\parallel} \approx 0.016$, as in the Pinsukanjana *et al.* (1992) experiment, the standing plasmons couple too weakly to be visible. It is also interesting to note that absorption peaks corresponding to single-particle transitions, if present, are also too weak to be seen (unless one regards the Kohn-theorem, sloshing or centre-of-mass mode as a coalescence of depolarisation-shifted single-particle transitions). Next consider the WPQW dispersion curves (Fig. 12). Arrows on the q_{\parallel} axis indicates the first two grating coupler wavenumbers q_n for a grating of spatial period 4×10^{-6} m, the value used in the experimental data of Pinsukanjana *et al.* (1992). The dispersion curves show that the centre-of-mass mode frequency does indeed approach $\omega_p = 0.333$ a.u.* as $q_{\parallel} \rightarrow 0$, in agreement with Kohn's theorem. They also show (in conjunction with the mode profile data not given here) that the hydrodynamic model of Section 2 was correct in predicting that the '2D plasmon' behaves like an even combination of surface plasmons at large q_{\parallel} .

The modified parabolic-linear wells (open symbols in Figs 10a and 10d) are predicted to have a richer absorption spectrum than the strictly parabolic wells. The '2D plasmon' peak is present as required by the theorem of Section 5. Kohn's theorem does not apply but there are resonances in the general vicinity of ω_p for small q_{\parallel} . These are presumably 'interband' modes in the terminology of Stern (1967) and Das Sarma (1984). In the present wells there is considerable 'depolarisation shifting' plus coupling among interband resonances and between interband and intraband resonances, so that this type of classification is not as clearcut as it is for the heterojunction wells discussed e.g. by Das Sarma (1984). In those cases the very uneven spacing of energy levels ϵ_i allowed a clear distinction between different interband modes, not available in parabolic-type wells because of the nearly even energy level spacing of the higher levels in the latter. At least one of the additional modes is best described, in the author's opinion, as a multipole surface plasmon. For neutral linear-parabolic wells this mode appears, for all well widths studied numerically including cases not shown here, at about $0.8 \omega_p$ (middle peak, squares, Figs 10a and 10c). Its mode profile (Fig. 11c) is neutral separately at each electron gas surface, just as for the multipole surface plasmon on simple metals (Dobson and Harris 1988; Tsuei *et al.* 1991). There is no such mode on the pure parabolic wells, presumably because of their narrower 'embedded electron gas' surface density profile (see the argument in Section 3 and Dobson 1992). The linear parabolic well also shows standing plasmon resonances (data not shown here), but their strength is distributed differently, as a function of q_{\parallel} , from those of the WPQW[†].

[†] (Note added in proof). On the linear-parabolic wells it does not seem possible to distinguish single-particle effects induced by boundary conditions from the weak standing plasmons which might be present (Schaich, W. L., and Dobson, J. F., to be published).

8. Summary, Conclusions, Future Directions

We have stressed that the infrared response of parabolic $\text{Ga}_{1-x}\text{Al}_x\text{As}$ wide parabolic quantum wells (WPQWs) is roughly, but not exactly, equivalent to the response of jellium slabs whose thickness can be varied, by gate bias, from the 2D to the 3D regime. Linear-lipped parabolic wells (LPQWs) are better jellium slab analogues, better in fact than simple metal samples. This is because, provided the band effective mass m^* and semiconductor dielectric constant ϵ are taken into account, the discrete-lattice effects in $\text{Ga}_{1-x}\text{Al}_x\text{As}$ are much smaller than those in simple metals.

The WPQW, when excited in an IR grating coupler experiment at low surface-parallel wavenumber, has two strong absorptions which can be understood as even and odd combinations of surface charge oscillations, or equivalently as low-frequency longitudinal (intraband) plasmon and high-frequency transverse (interband) centre-of-mass sloshing modes. The low-frequency mode has the same $\sqrt{q_{\parallel}}$ dispersion as a 2D plasmon, a result proved in Section 3 to hold for all quantum wells at low enough q_{\parallel} . (For wide wells, despite its dispersion, this mode is not really two-dimensional, charge perturbation occurring disjointly at the two surfaces: see Fig. 11a.) The upper mode appears to be continuous, as $q_{\parallel} \rightarrow 0$, with the Kohn-theorem mode described in Section 3, and so occurs close to the ‘bulk’ plasma frequency ω_p . Additional single-particle transition peaks appear both from experiment and theory to be weak or nonexistent in this regime. Thus to a first approximation the WPQW resonance frequencies at low q_{\parallel} are completely described by theorems without the need for numerical calculation. While disappointing from a many-body theorist’s viewpoint, this stability of the mode frequencies might be useful in device applications.

At higher q_{\parallel} the grating-coupled WPQW (like the regular jellium slab) is predicted to show measurable absorption peaks above ω_p which are due to standing bulk plasmons fitting across the electron layer (see footnote on preceding page). The spacing and q_{\parallel} dispersion of these peaks do show many-body effects and it would be particularly interesting to observe these for shallower parabolic wells ($5 < r_s^* < 6$), in view of the anomalous results obtained experimentally (vom Felde *et al.* 1989) for the bulk plasmon dispersion in cesium. Very accurate measurements of the dispersion of the ‘2D plasmon’ mode of WPQWs could also shed light on many-body effects, since the first correction to the $\sqrt{q_{\parallel}}$ dispersion is sensitive to these (Beck and Kumar 1976; Dahl and Sham 1977; Batke *et al.* 1986). Small observed anomalies (Pinsukanjana *et al.* 1992) in the upper (centre-of-mass) mode frequency of WPQWs as a function of gate bias may reflect genuine many-body effects dependent on layer thickness (Das Sarma *et al.* 1990), but could also be related to inhomogeneous m^* and ϵ values (Das Sarma 1992, personal communication).

The transition of the grating-coupled IR spectrum of WPQWs from the 2D limit ($L \rightarrow 0$) to the 3D limit ($L \rightarrow \infty$) proceeds as follows. The two strong low- q_{\parallel} resonances coalesce at larger values of $q_{\parallel} L$, to even and odd 3D *surface* plasmons. It is the standing plasmon modes, very weakly excited in grating experiments at low q_{\parallel} , which become bulk plasmons in the limit $L \rightarrow \infty$.

Linear-parabolic wells (LPQWs), when correctly filled with electrons, are a better approximation to neutral jellium slabs than are the pure WPQWs. LPQWs are predicted to have additional resonance lines at low q_{\parallel} , compared

with the WPQW. For narrow slabs some of these are shifted single-particle transitions, but for all widths the theory shows a ‘multipole surface plasmon’ (MSP) peak (Dobson 1992; Tsuei *et al.* 1991) at about $0.8 \omega_p$, whose absence on the pure WPQW can be understood in hydrodynamic terms as arising from the more steeply-falling static surface electron density profile in the WPQW. (The term ‘multipole *surface* plasmon’ should not be confused with the term ‘multipole excitation’ used by some authors to describe any resonance due to single-particle transitions between different well eigenstates or sub-bands.) In the WPQW the electron gas edge is qualitatively different from that in a neutral jellium slab, being ‘embedded’ inside the jellium background (see Dobson 1992). Theory suggests that the MSPs in linear–parabolic wells can be switched on or off by a modest gate bias variation, pulling the electron gas edge on or off the edge of the effective positive background from the ‘regular’ to the ‘embedded’ edge configuration. Such a switching effect might have technological uses. The understanding of edge effects gained here may be useful in other systems such as quantum dots.

Acknowledgments

I would like to acknowledge useful discussions or communications with E. Gwinn, K. Ennslin, A. Wixforth, W. Kohn, A. MacDonald, W. Schaich, E. Gross, C. Dharma-Wardana, S. Das Sarma, D. Neilson, F. Green, J. Mahanty and M. Das. The hospitality of the School of Physics, University of New South Wales was also much appreciated.

References

- Ando, T. (1977) *Z. Phys.* B **26**, 263.
 Bastard, G. (1981). *Phys. Rev.* B **24**, 5693.
 Batke, E., Heitmann, D., and Tu, C. W. (1986). *Phys. Rev.* B **34**, 6951.
 Becke, D. E., and Kuma, P. (1976). *Phys. Rev.* B **13**, 2859 (erratum *ibid.* p. 5127).
 Bennett, A. J. (1970). *Phys. Rev.* B **1**, 203.
 Brey, L., Johnson, N. F., and Halperin, B. I. (1989). *Phys. Rev.* B **40**, 10647.
 Burt, M. G. (1992). *J. Phys. Condens. Matt.* **4**, 6651.
 Ceperley, D. M., and Alder, B. J. (1980). *Phys. Rev. Lett.* **45**, 566.
 Dahl, D. A., and Sham, L. J. (1977). *Phys. Rev.* B **16**, 651.
 Das Sarma, S. (1984). *Phys. Rev.* B **29**, 2334.
 Das Sarma, S., Jalabert, R., and Yang, S.-R. E. (1990). *Phys. Rev.* B **41**, 8288.
 Das Sarma, S., and Quinn, J. J. (1979). *Phys. Rev.* B **20**, 4872.
 Dobson, J. F. (1992). *Phys. Rev.* B **46**, 10163.
 Dobson, J. F., and Harris, G. H. (1983). *Phys. Rev.* B **27**, 6542.
 Dobson, J. F., and Harris, G. H. (1986). *J. Phys.* C **19**, 3971.
 Dobson, J. F., and Harris, G. H. (1988). *J. Phys.* C **21**, L729.
 Dobson, J. F., and Harris, G. H. (1990). *J. Phys. Condens. Matt.* **2**, 6461.
 Dobson, J. F., and Rose, J. H. (1982). *J. Phys.* C **18**, 7429.
 Dreizler, R. M., and Gross, E. K. U. (1990). ‘Density Functional Theory’ (Springer: Berlin).
 Eguiluz, A. (1979). *Phys. Rev.* B **19**, 1689.
 Eguiluz, A. G. (1983). *Phys. Rev. Lett.* **51**, 1907.
 Eguiluz, A., and Quinn, J. J. (1976). *Phys. Rev.* B **14**, 1347.
 Eguiluz, A., Ying, S. C., and Quinn, J. J. (1975). *Phys. Rev.* B **11**, 2118.
 Fasol, G., King-Smith, R. D., Richards, D., Ekenberg, U., Mestres, N., and Ploog, K. (1989). *Phys. Rev.* B **39**, 12695.
 Feibelman, P. J. (1971). *Phys. Rev.* B **3**, 220.
 Feibelman, P. J. (1982). *Prog. Surf. Sci.* **12**, 287.

- Green, F., Neilson, D., and Szymanski, J. (1985). *Phys. Rev. B* **31**, 2796.
- Gross, E. K. U., and Kohn, W. (1985). *Phys. Rev. Lett.* **55**, 2850 [erratum *ibid.* (1986) **57**, 923].
- Gwinn, E., Westervelt, R. M., Hopkins, P. F., Rimberg, R. M., Sundaram, M., and Gossard, A. C. (1989). *Phys. Rev. B* **39**, 6260.
- Harris, J., and Griffin, A. (1971). *Phys. Lett. A* **34**, 51.
- Iwamoto, N., and Gross, E. K. U. (1987). *Phys. Rev. B* **35**, 3003.
- Jackson, J. D. (1962). 'Classical Electrodynamics' (Wiley: New York).
- Kempa, K., Broido, D. A., Beckwith, C., and Cen, J. (1989). *Phys. Rev. B* **40**, 8385.
- Kohn, W. (1961). *Phys. Rev.* **123**, 1242.
- Kohn, W., and Sham, L. J. (1965). *Phys. Rev.* **140**, A1133.
- Lang, N. D. (1973). *Solid State Phys.* **28**, 225.
- Lang, N., and Kohn, W. (1970). *Phys. Rev. B* **1**, 4555.
- Liebsch, A. (1987). *Phys. Rev. B* **36**, 7378.
- Mahan, G. D. (1981). 'Many Particle Physics' (Plenum: New York).
- Mahanty, J. (1982). *Aust. J. Phys.* **35**, 147.
- Pinsukanjana, P. R., Gwinn, E. G., Dobson, J. F., Yuh, E. L., Asmar, N. G., Sundaram, M., and Gossard, A. C. (1992). *Phys. Rev. B* **46**, 7284.
- Ritchie, R. H. (1957). *Phys. Rev.* **106**, 874.
- Rose, J. H., and Dobson, J. F. (1991). *Solid State Commun.* **37**, 91.
- Schwartz, C., and Schaich, W. L. (1982). *Phys. Rev. B* **26**, 7008.
- Schwartz, C., and Schaich, W. L. (1984). *Phys. Rev. B* **30**, 1059.
- Stern, F. (1967). *Phys. Rev. Lett.* **18**, 546.
- Stern, F., and Das Sarma, S. (1984). *Phys. Rev. B* **30**, 840.
- Sundaram, M., Gossard, A. C., English, J. H., and Westerveld, R. M. (1988). *Superlattices Microstructures* **4**, 683.
- Tsuei, K. D., Plummer, E. W., Liebsch, A., Pehlke, E., Kempa, K., and Bakshi, P. (1991). *Surf. Sci.* **247**, 302.
- vom Felde, A., Sprosser-Prou, J., and Fink, J. (1989). *Phys. Rev. B* **40**, 10181.
- Zangwill, A., and Soven, P. (1980). *Phys. Rev. A* **21**, 1561.
- Zheng, L., and Schaich, W. L. (1991). *Phys. Rev. B* **43**, 4515.
- Zheng, L., Schaich, W. L., and MacDonald, A. H. (1990). *Phys. Rev. B* **41**, 8493.